BROADBAND MODE DECOMPOSITION OF DUCTED FAN NOISE USING CROSS-SPECTRAL MATRIX DENOISING

Arthur FINEZ[1], Antonio PEREIRA[2], Quentin LECLERE[2]

[1] MicrodB, *28 chemin du petit bois - 69134 Ecully Cedex - France*

[2] Laboratoire Vibrations Acoustique, *25 bis av. Jean Capelle - 69621 Villeurbanne cedex - France*

SUMMARY

Ducted fan mode decomposition in the broadband frequency range requires advanced denoising techniques of microphone surface pressure measurements to get rid of the wall duct turbulent boundary layer noise. Three new denoising techniques are presented in this study, compared using simulations and applied to ducted fan measurements. The simulations assume a specific duct mode loading and additional white noise is added raising a -10 dB Signal-to-Noise Ratio. The experiment concerns a ducted ventilation fan rotating at 10 000 rpm and the azimuthal and axial mode decomposition is applied up to a reduced frequency of kr = 7.5. It is shown numerically and experimentally that two denoising approaches enhance the modal identification results, improving significantly the dynamic range of the method.

INTRODUCTION

In the prospect of classifying ducted fan broadband noise sources, an accurate description of the acoustic pressure field in the duct is required. Thanks to the duct propagation characteristics the acoustic energy is carried only by a finite number of orthogonal modes at a given frequency, so that the determination of a few number of unknowns allows to characterize perfectly the acoustic field at a sufficient distance from the sources.

Whereas tonal noise mode decomposition is widely studied in the literature, there are few measurement techniques dedicated to broadband noise. Such a technique has been described by Enghardt & al. [1]. They use duct surface pressure measurements to compute azimuthal and radial mode coefficients by means of an inverse method. They used cross-correlation between a reference microphone and wall flush-mounted microphones. Making the assumption that the modes are fully

uncorrelated allows to compute both downstream and upstream propagating mode coefficients. Castres and Joseph [2] presented a technique to compute the mode coefficients on the basis of an external spherical array. In such a configuration, the microphone data are not polluted by the internal noise which enables to use the whole measurement cross-spectral matrix as input for the inverse method. There is no assumption on the mode correlation and the mode coherence can be estimated.

In the present paper it is proposed to use a general technique similarly to Castres and Joseph using an in-duct flush-mounted microphone array. The main difficulty arises from the turbulent boundary layer (TBL) on the duct inner surface. The pseudo-noise mean square pressure at the microphone location is at least 10 dB higher than the acoustic one. The raw cross-spectral matrix diagonal is dominated by the pseudo-noise as well as possibly some off-diagonal terms if the microphone spacing is smaller than the TBL correlation length. As a consequence, a matrix denoising step is applied before the mode resolution method and is the main focus of this study.

Indeed, the problem of separating the acoustical part from the hydrodynamic part (or merely suppressing the flow noise) of surface pressure measurements under a TBL was firstly studied in the late 1970's. Chung [3] has proposed a technique based on the ordinary coherence functions of three transducers to extract the part of the auto-spectrum as received by the sensors without the flow. The performance of such technique is expected to decrease as the number of independent sources is increased and the mutual coherence of different transducers is low. Other methods have been proposed since then, for instance a subspace approach [4] based on a Generalized Singular Value (GSVD) decomposition, a separation based on a wavenumber representation of the surface pressure measurements [5] or a separation based on an energetic partitioning using a Principal Component Analysis (PCA) [6].

In this paper, three different techniques aiming to suppress the noise due to the TBL on in-duct pressure measurements are presented and compared. Numerical simulations are used as a comparison basis and the methods are then applied to real data. The final goal is to assess the information from a broadband modal decomposition technique without the influence of the strong flow noise, which largely predominates on the broadband component of the measured acoustic pressure.

IN-DUCT MEASUREMENT METHODS

Modal Decomposition (MD) Method

The modal decomposition method consists in the reconstruction of modal duct weights from pressure surface measurement. In the case of an infinite cylindrical duct, each mode is characterized by the double index (m,n), respectively the azimuthal and the radial mode order. Following Goldstein [7], the acoustic field in a duct of circular cross-section may be expressed as a sum of modal components:

$$p(r,\theta,z) = \sum_{m=-\infty}^{+\infty} \sum_{n=1}^{+\infty} \left(\alpha_{mn} e^{-i\gamma_{mn}^{+}(z-z_0)} + \beta_{mn} e^{+i\gamma_{mn}^{-}(z-z_0)}\right) \psi_{mn}(r,\theta) \tag{1}$$

where $p(r,\theta,z)$ is the acoustic pressure to be measured at the duct radius $r = a$, α_{mn} and β_{mn} are the downstream and upstream-traveling mode coefficients (to be evaluated in an arbitrary reference plane $z=z_0$), ψ_{mn} is the set of modal shape functions, γ_{mn}^{+} and γ_{mn}^{-} are the axial wave number in the positive and negative axial direction. For the sake of clarity only the downstream propagating modes are considered in this study, so β_{mn} is set to 0, even if the method can deal with both direction without modification. Sources are thus assumed to be on the negative z direction of the infinite duct. Note however that adding the back-propagating modes would divide the maximum analysis frequency by a factor 2.

At a given frequency, only a finite number of γ_{mn}^{+} have a zero imaginary part, so that there are only a few number of propagating modes to be solved. Restricting equation (1) to those modes allows to express the system in matrix form

$$\mathbf{P} = \boldsymbol{\psi}\,\boldsymbol{\alpha} \tag{2}$$

where $\mathbf{P}$ is the vector of measured complex pressure at the array microphone locations, $\boldsymbol{\alpha}$ is the unknown vector of cut-on mode amplitudes and $\boldsymbol{\psi}$ is the mode-microphone transfer matrix expressed from equation (1).

In the broadband frequency range, it is useful to work with the cross-spectral matrix (CSM) $\boldsymbol{S_{pp}} = \lim_{T\to\infty} E(\frac{1}{T}\mathbf{P}\mathbf{P}^{\mathbf{H}})$ and the mode covariance matrix $\boldsymbol{S_{\alpha\alpha}} = \lim_{T\to\infty} E(\frac{1}{T}\boldsymbol{\alpha}\boldsymbol{\alpha}^{\mathbf{H}})$ containing both the mode amplitude and coherence information. Equation (2) can then be restated as

$$\boldsymbol{S_{pp}} = \boldsymbol{\psi}\,\boldsymbol{S_{\alpha\alpha}}\,\boldsymbol{\psi}^{\mathbf{H}}. \tag{3}$$

The least mean square solution of eq. (3) $\widehat{\boldsymbol{S}}_{\boldsymbol{\alpha\alpha}}$ can be found using the pseudo-inverse of the transfer matrix $\boldsymbol{\psi}^{\dagger} = (\boldsymbol{\psi}^{\mathbf{H}}\boldsymbol{\psi})^{-1}\,\boldsymbol{\psi}^{\mathbf{H}}$

$$\widehat{\boldsymbol{S}}_{\boldsymbol{\alpha\alpha}} = \boldsymbol{\psi}^{\dagger}\,\boldsymbol{S_{pp}}\,\boldsymbol{\psi}^{\mathbf{H}\dagger}. \tag{4}$$

The square matrix $\widehat{\boldsymbol{S}}_{\boldsymbol{\alpha\alpha}}$ provides an estimate of the modal covariance matrix, the diagonal term represents the mode energy and the off-diagonal the coupling between two modes. The sensitivity of the inversion to the measurement noise depends on the condition number of the matrix $\boldsymbol{\psi}$. If the inversion is unstable, a dedicated regularization procedure is needed. The double ring array used in the present application is sketched on Figure 1. The condition number is plotted against the reduced frequency ka (a being the duct radius) and is sufficiently low up to a critical frequency $ka = 7$ corresponding to the cut-on frequency of the (0,3) mode. In this study, the critical frequency range is taken lower than 7 so that no regularization is needed. The whole mode decomposition procedure has been validated against numerical simulation using the ACTRAN commercial software.

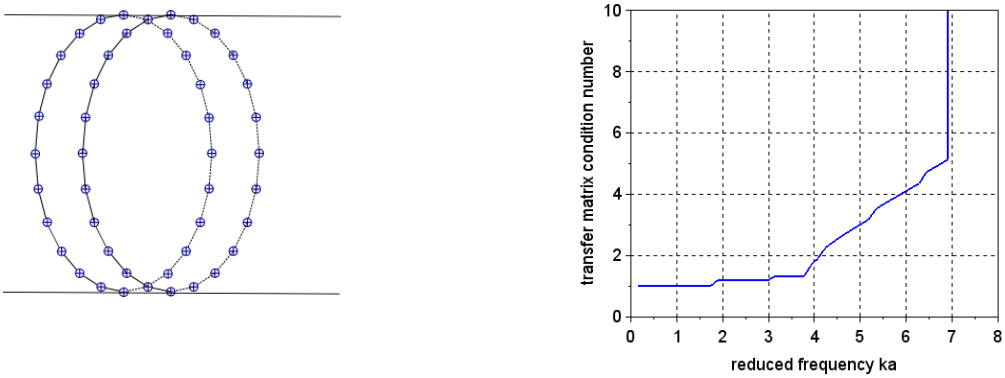

Figure 1: left: flush-mounted 48 microphone locations,
right: condition number of matrix $\boldsymbol{\psi}$ as a function of reduced frequency.

Denoising Techniques

Diagonal Reconstruction (DR)

In the context of flush-mounted aeroacoustic measurements, the boundary layer noise contamination is a standard problem and is generally dealt with by setting the CSM diagonal to zero[8]. This technique is known to increase the dynamic range of standard localization methods like beamforming. However if applied to the present mode decomposition method, output mode amplitudes may be

negative because the new CSM is not physical. A new method is proposed here consisting in reconstructing the CSM diagonal from off-diagonal values. The principle is to seek microphone autospectra that are compatible with all measured cross-spectra. In this denoising technique it is assumed that the TBL correlation length is much smaller than the minimum microphone spacing so that the contamination only affects the autospectra and not the off-diagonal elements of the CSM.

The main assumption is that the acoustic field is perfectly coherent between pairs of microphone while the contamination noise is not coherent. In other terms, if S_{ij} denotes the measured cross-spectrum between microphone i and j and $\tilde{S}_{ii}$ the new estimated auto-spectrum, it is assumed that:

$$\forall\, i \neq j, \qquad \gamma_{ij}^2 = \frac{|S_{ij}|^2}{\tilde{S}_{ii}\tilde{S}_{jj}} = 1. \tag{5}$$

Using the logarithmic notation, equation (5) reads in matrix form:

$$\mathbf{L} = \mathbf{M}\,\mathbf{A}. \tag{6}$$

Considering M microphones, $\mathbf{L}$ is a column vector of $M\,(M-1)/2$ elements which are equal to $20\log_{10}|S_{ij}|$, using an adequate pair numbering, $\mathbf{A}$ is a $[M\,,1]$ vector of $10\log_{10} S_{ii}$ elements, and the $\left[\frac{M\,(M-1)}{2}, M\right]$ $\mathbf{M}$ matrix and its pseudo-inverse $\mathbf{M}^{\dagger}$ can be written explicitly:

$$\mathbf{M} = \begin{bmatrix} 1 & 1 & 0 & 0 & \dots & 0 \\ 1 & 0 & 1 & 0 & \dots & 0 \\ 1 & 0 & 0 & 1 & \dots & 0 \\ \vdots & \vdots & \vdots & \vdots & \vdots & \vdots \\ 1 & 0 & 0 & 0 & \dots & 1 \\ 0 & 1 & 1 & 0 & \dots & 0 \\ 0 & 1 & 0 & 1 & \dots & 0 \\ \vdots & \vdots & \vdots & \vdots & \vdots & \vdots \\ 0 & 0 & 0 & \cdots & 1 & 1 \end{bmatrix} \tag{7},$$

$$\mathbf{M}^{\dagger} = \begin{bmatrix} \zeta & \zeta & \cdots & \zeta & \chi & \chi & \cdots & \chi \\ \zeta & \chi & \cdots & \chi & \zeta & \zeta & \cdots & \vdots \\ \chi & \zeta & \cdots & \vdots & \zeta & \chi & \cdots & \vdots \\ \vdots & \chi & \cdots & \vdots & \chi & \zeta & \cdots & \chi \\ \vdots & \vdots & \cdots & \chi & \vdots & \chi & \cdots & \zeta \\ \chi & \chi & \cdots & \zeta & \chi & \vdots & \cdots & \zeta \end{bmatrix} \tag{8}$$

where $\zeta = 1/(M-1)$ and $\chi = -1/((M-1)(M-2))$. The system of equation (6) is over determined as long as $M > 3$. Note that the only dependence of matrix $\mathbf{M}$ and $\mathbf{M}^{\dagger}$ against the setup is the number of microphone M. The condition number is lower than 2 even with a small number of microphones, so that equation (6) can be solved in the least mean square sense again without regularization and elements of $\mathbf{A}$ can be estimated from the cross-spectra through the direct equation $\widetilde{\mathbf{A}} = \mathbf{M}^{\dagger}\,\mathbf{L}$ which leads to the estimated autospectra $\tilde{S}_{ii}$.

Alternate Projections (AP)

In this section we describe an approach based on the concept of alternating projections [8,9], which is an iterative technique used to find the intersection of a given number of convex sets. Two sets are defined here with different purposes. The first is the set of positive semi-definite matrices, which is inherent to the definition of cross spectral matrices. The second set results from a projection onto a spatial basis, with the aim to encode the structure information to the cross-spectral matrix. The purpose of the second projection is to take into account the eventual spatial coherence of the acoustic field.

In other words, the first projection introduces a statistical information to the reconstructed matrix and the second endows a spatial information. The choice of the basis for the spatial projection is closely related to the experimental configuration (geometry of the array, shape of the source field, type of acoustic propagation). A direct choice for the case of in-duct measurements is the modal basis which describe the acoustic field inside the duct.

Sparse & Low-Rank Decomposition (SLRD)

The third approach studied here is based on a decomposition of the measured cross spectral matrix into two parts, the first carrying the acoustical information and the second carrying the noise related to turbulent boundary layer. The decomposed cross spectral matrix is written as follows:

$$\boldsymbol{S_{pp}} = \mathbf{L} + \mathbf{S}, \tag{9}$$

where **L** is a low rank matrix and **S** a sparse matrix. The assumption of a low-rank matrix is justified by the fact that only a finite number of uncorrelated modes contribute to the acoustic energy at a given frequency. The sparse property of the matrix **S** means that it has only few non-zero entries. This is a plausible assumption if we consider that the correlation length of a TBL is sufficiently small and thus the noise is concentrated mainly on the autospectra, i.e. diagonal of the CSM. The recovery of **L** can be formulated by the following minimization problem [10,11]:

$$\text{minimize } \| \mathbf{L} \|_* + \lambda \| \mathbf{S} \|_1 \qquad \text{subject to } \mathbf{L} + \mathbf{S} = \mathbf{S_{pp}} \tag{10}$$

where $\|\cdot\|_*$ is the nuclear norm (given by the sum of the singular values of a matrix), $\|\cdot\|_1$ is the l_1-norm (sum of absolute values of all entries) and λ a regularization parameter, which controls the weight on the sparse term. This problem may be efficiently solved by an accelerated proximal gradient algorithm [10]. Similarly to the previous method, although in a second step here, a projection onto a spatial basis is introduced to encode a spatial information/structure on the solution. The choice of a regularization parameter λ is of importance to balance the weight on the sparse part, and a value $\lambda = 0.1$ is used throughout this work.

Remarks on denoising techniques

In this section we summarize the basic assumptions and characteristics of the techniques presented above. The Diagonal Reconstruction method assumes that the acoustic field is perfectly coherent and the noise due to the TBL is not coherent between neighboring microphones. The method thus seeks to reconstruct the autospectra which maximize the coherence between microphones, and contrary to the other two methods, does not modify the cross-spectra. The technique based on alternate projections only forces the reconstructed matrix to be positive semi-definite and uses the modal behavior of the pressure field inside the duct. No hypothesis concerning the spatial correlation of the TBL field is made. The third method makes the assumption that the CSM may be decomposed into a low-rank part (assuming that only few acoustic modes are excited at a given frequency) and a sparse part, which in turn assumes that only few entries are corrupted by strong noise, in the studied case, mainly the diagonal of the matrix. The latter assumption is expected to be less valid in the presence of a disturbing noise with a spatial correlation higher than the inter-microphone spacing. In terms of computational time, the diagonal reconstruction has the best performance, since it is based on a pseudo-inversion which may be written explicitly, contrary to the other two methods which depend on an iterative procedure.

NUMERICAL VALIDATIONS

Signal generation

The numerical simulations are realized according to different cases concerning the modal correlation. Three cases are defined : (a) uncorrelated modal components; (b) correlated modal components and (c) partially correlated modes. The aim is to evaluate the ability of the inverse method to identify not only the modal amplitudes but a possible correlation between modes.

Following the nomenclature from previous sections, the complex acoustic pressure received at the microphones may be written as

$$\mathbf{p} = \boldsymbol{\psi}\mathbf{s}, \tag{11}$$

where $\mathbf{s}$ is a vector of complex modal amplitudes. In order to introduce a possible correlation between modes, $\mathbf{s}$ is seen as a realization (named hereafter a snapshot) from a multivariate random process distributed according to $\mathbb{C}\boldsymbol{\mathcal{N}}_k(\boldsymbol{\mu}, \boldsymbol{\Sigma})$, which is a multivariate complex Gaussian distribution of dimension k, mean vector $\boldsymbol{\mu}$ and covariance matrix $\boldsymbol{\Sigma}$. Throughout the simulations it is assumed that $\boldsymbol{\mu} = 0$ and the covariance matrix is modeled according to the three following cases:

(a) Uncorrelated case : $\boldsymbol{\Sigma} = \mathbf{I}_\mathrm{K}$, with $\mathbf{I}_\mathrm{K}$ the identity of dimension K
(b) Fully correlated case : $\boldsymbol{\Sigma}_{\mathrm{i,k}} = 1 \ \forall \, \mathrm{i, k}$
(c) Partially correlated case : $\boldsymbol{\Sigma}_{\mathrm{i,k}} = 0.5 \ \forall \, \mathrm{i} \neq \mathrm{k}$ and $\boldsymbol{\Sigma}_{\mathrm{i,k}} = 1 \ \forall \, \mathrm{i} = \mathrm{k}$

Noise is then added to the simulated acoustic pressure directly to the snapshots, hence we have for the i-$^{\mathrm{th}}$ snapshot:

$$\mathbf{p}_{(\mathrm{i})} = \boldsymbol{\psi}\mathbf{s}_{(\mathrm{i})} + \mathbf{n}_{(\mathrm{i})}, \tag{12}$$

where $\mathbf{n}$ is also distributed according to $\mathbb{C}\boldsymbol{\mathcal{N}}_M(\mathbf{0}, \sigma^2\boldsymbol{\Omega}_\mathrm{M})$, with σ^2 the noise energy which is proportional to the signal-to-noise ratio (SNR). Note here that the random vector is M-dimensional, M being the number of microphones. Two cases are defined below for the covariance matrix of noise $\boldsymbol{\Omega}_\mathrm{M}$. Firstly it is assumed that the noise is uncorrelated between microphones (i.e. $\boldsymbol{\Omega}_\mathrm{M} = \mathbf{I}_M$) and in a second time, an empirical model for the noise due to a turbulent boundary layer (TBL) is used to define a new covariance matrix. An estimate of the noisy CSM is obtained by averaging the simulated pressure vectors over several snapshots:

$$\hat{\mathbf{S}}_{\mathrm{pp}} = \frac{1}{\mathrm{N_s}} \sum_{\mathrm{i}=1}^{\mathrm{N_s}} \mathbf{p}_{(\mathrm{i})} \mathbf{p}_{(\mathrm{i})}{}^{H}, \tag{13}$$

with $\mathrm{N_s}$ the number of snapshots. As discussed in the introduction, if the correlation length related to the TBL is smaller than the microphone spacing, the hydrodynamic noise is mainly concentrated on the diagonal of the CSM. The effect of the averaging process on Eq. (13) is such that the noise will be predominantly loaded on the autospectra, but still a residual noise will remain on the cross-spectra. The simulations may thus be seen as a good approximation of the reality.

In the following simulations, the number of snapshots is 200 and the SNR is equal to -10 dB. The loaded modes are (0,1), (1,1), (-1,1) with a unit amplitude.

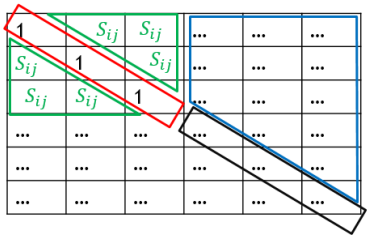

Figure 2: Estimated mode covariance matrix $\widehat{\boldsymbol{S}}_{\boldsymbol{\alpha\alpha}}$ with the values taken for the comparison criteria. Loaded modes are supposed to be the three first modes (upper-left part of the matrix).

Comparison Criteria

To quantify the ability of each denoising technique to clean the CSM as an input for the modal decomposition method, four indicators are computed from the estimated output mode covariance matrix $\widehat{\boldsymbol{S}}_{\boldsymbol{\alpha\alpha}}$. These indicators are compared to the expected "no-noise" values; their description here below refers to values denoted on Figure 2:

1. the autospectrum level of the each loaded mode (red color on Figure 2). In the present work, the theoretical value is 1,

2. the maximum autospectrum value of not-loaded modes (black color on Figure 2). In case of success, this indicator should be equal to 0,
3. mean coherence between loaded modes, computed from cross-spectra in green color on Figure 2. The expected value is 0 in case of uncorrelated modes, 1 in case of a full correlation between modes, and 0.5 in case of partially correlated modes,
4. mean residual cross-spectra (blue color on Figure 2). Note that this indicator includes both correlation between to two idle modes, and residual correlation between one loaded mode and one idle mode. In any case, the expected value is 0.

For each denoising technique, these four quality criteria are plotted and compared as a function of the frequency.

Uncorrelated Modes Results

The first simulation deals with the case of perfectly uncorrelated modes with a SNR = -10 dB. On Figure 3 the autospectra of two loaded modes are shown (indicator #1). The reference curve (red) is very close to unity for the (0,1) mode up to 4466 Hz. The following analysis can explain this observation: the sensor azimuthal spacing is useful for the azimuthal mode discrimination while the sensor axial spacing is useful for the radial mode discrimination. Since the current array is made of only two axially separated rings, the technique is unable to distinguish between modes (0,1), (0,2) and (0,3) above the (0,3) cut-on frequency which corresponds to $f_c^{(0,3)} = 4466$ Hz (with a duct radius $a = 0.085$ m).

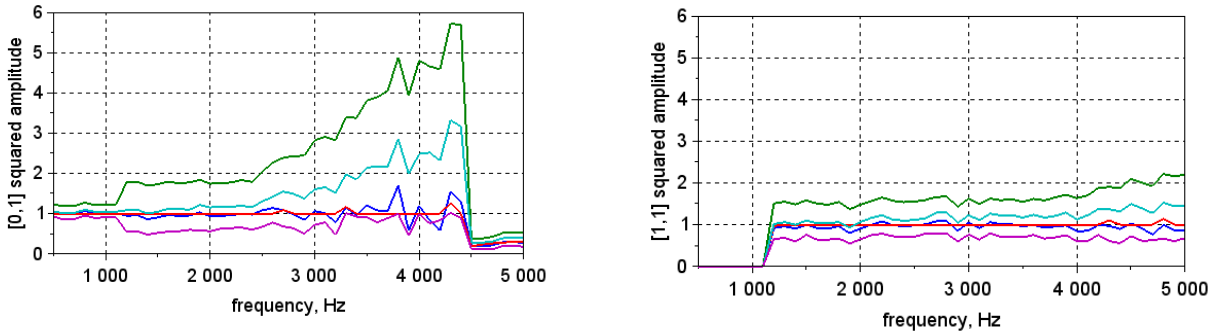

Figure 3: Autospectra of loaded mode (0,1) left and (1,1) right, output from the mode decomposition procedure with several denoising techniques previously applied on the CSM. Red: no-noise reference; green: noisy raw CSM; dark blue: DR method; light blue: AP method; magenta: SLRD method.

The noisy case shows that mode (0,1) is strongly overestimated if no denoising technique is applied. All denoising techniques provide enhanced results compared to the noisy case, especially the DR method.

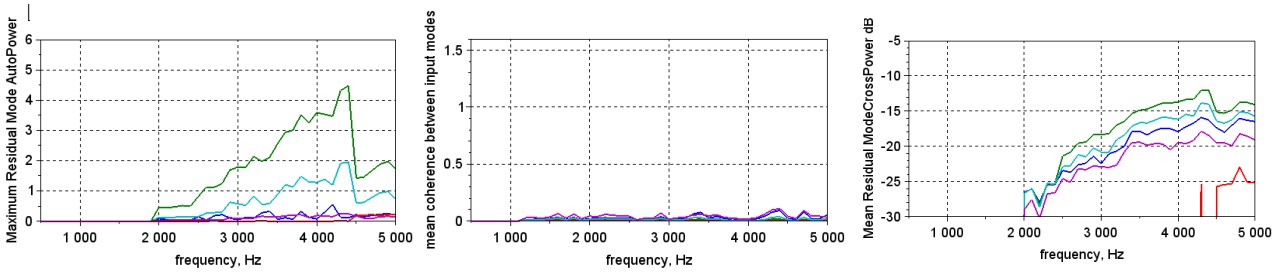

Figure 4: Indicators #2 (left), #3 (center), #4 (right) for the uncorrelated mode case. Red: no-noise reference; green: noisy raw CSM; dark blue: DR method; light blue: AP method; magenta: SLRD method.

Concerning the (1,1) mode case it can be observed that the reconstructed amplitude is null for $f < f_c^{(1,1)} = 1172$ Hz which is not surprising since this mode is cut-off below this frequency.

Above 1172 Hz, best results are also obtained with the DR method. Similar results are obtained for the (-1,1) mode.

On Figure 4 the MD technique applied to the noisy CSM attributes high amplitudes on idle modes (green curve on the left plot). This means that if no denoising is applied, the method is not able to correctly separate loaded and idle modes. DR and SLRD denoising methods provides satisfactory and equivalent results. The coherence (indic. #3 on center position) is equivalently found close to 0 for all methods, while residual mode crosspectra (indic. #4 on the right hand side) is minimized with SLRD method (not higher that -10 dB).

Correlated Modes Results

The second simulation concerns a similar test case with SNR = -10dB; however a perfect correlation between loaded modes is introduced. Autospectra indicators (#1 and #2) are quite similar to the uncorrelated case and they are not shown here.

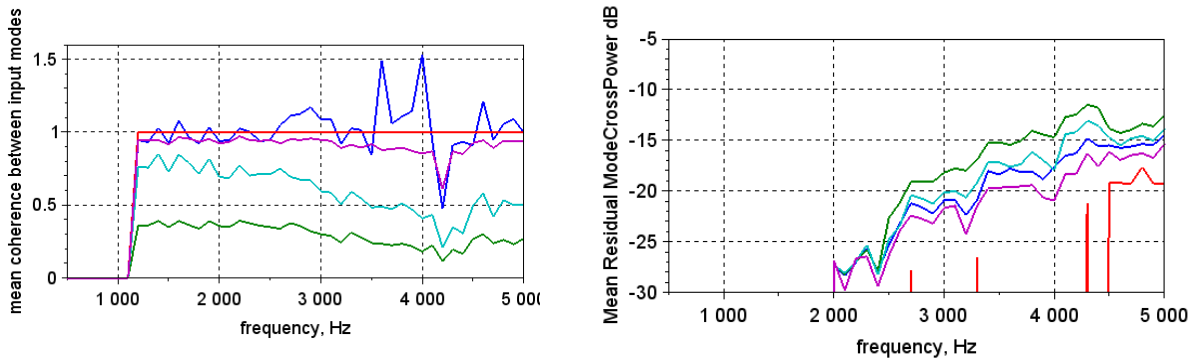

Figure 5: Indicator #3 (left), #4 (right) for the fully correlated mode case. Red: no-noise reference; green: noisy raw CSM; dark blue: DR method; light blue: AP method; magenta: SLRD method.

The off-diagonal indicators (#3 and #4) are shown on Figure 5. The mean coherence between input is expected to be equal to unity above $f_c^{(1,1)} = 1172$ Hz as occurs on the no-noise red curve. The noisy raw CSM exhibits a low coherence level around 0.25, while the SLRD method shows a mean coherence around 0,9 up to $f_c^{(0,3)} = 4466$ Hz. Note the case of the DR method which leads to an oscillating coherence curve centered on 1. However, certain values exceed unity. This is because the DR method only modifies the CSM diagonal values. The noise introduced on the off-diagonal elements is not corrected and this leads to a non semi-definite positive CMS and thus coherence values higher than 1. Concerning the mean residual crosspowers, the SLRD method implies again the lower values. It is seen here that the proposed techniques provide for the first time a tool to estimate the mode amplitude and correlation level from pressure measurement highly polluted by a turbulent boundary layer.

Partially Correlated Modes Results

In this third test, the mode loading is set to simulate a mode-to-mode correlation of 50% between input modes (0,1),(-1,1) and (1,1). Other modes amplitude are initially set to 0.

Figure 6 shows the off-diagonal indicator for this test case. Concerning the mean coherence between loaded modes, the noisy CSM induces low coherence level as in the fully correlated mode. The DR method provides a good estimate of the coherence with a variation of ± 10%. Surprisingly the SLRD provide coherence values with a bias, centered on 75%. For the indicator #4 as in other cases, the SLRD provides the lower residual levels.

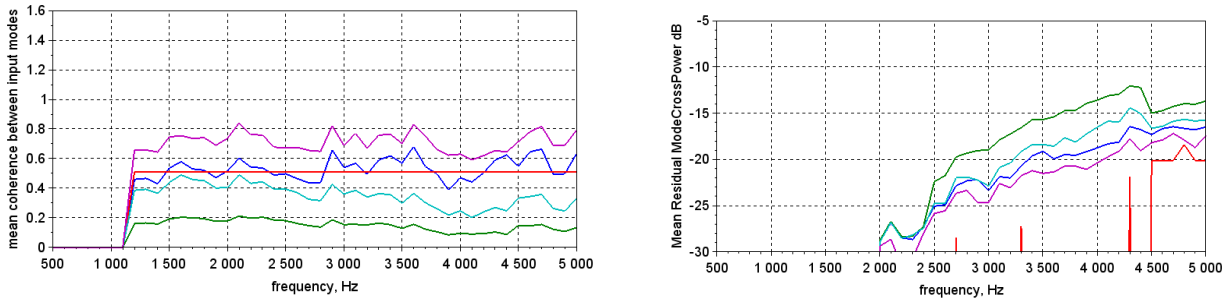

Figure 6: Indicator #3 (left), #4 (right) for the partially correlated mode case. Red: no-noise reference; green: noisy raw CSM; dark blue: DR method; light blue: AP method; magenta: SLRD method.

Locally Correlated Hydrodynamic Noise Results

In order to simulate a case more representative of the reality, a TBL model is used to introduce a spatial correlation on the flow noise. A Corcos model has been used to compute the coherence of neighboring microphones at each frequency. A flow convection velocity representative of the velocity expected on the experimental set-up presented on next section has been chosen. The same configuration as the previous section (modal correlation of 50%) is used here. The results are shown in Figure 7. In terms of modal amplitude, both DR and SLRD methods allow a good estimate for the whole frequency band under investigation. Similar results were found for the other 2 modes and are not shown here. Finally, the reconstructed coherence between modes is shown on Figure 7 (right panel). Results obtained are similar to the previous case when there was no spatial correlation on the perturbing noise. The SLRD method overestimates the coherence between modes and the DR method returns the best estimate.

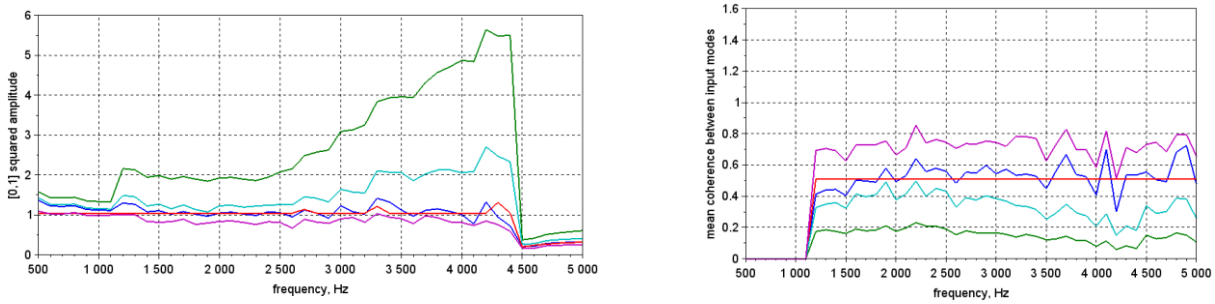

Figure 7: Indicator #1 (left) and #3 (right) for the locally correlated hydrodynamic noise case. Red: no-noise reference; green: noisy raw CSM; dark blue: DR method; light blue: AP method; magenta: SLRD method.

EXPERIMENTAL APPLICATION

Setup

Previous denoising methods are tested on a ducted ventilation fan of 17 cm diameter installed in the LMFA duct facility and shown on Figure 8. The rotation speed is set to 10000 rpm and no pressure valve is used. The rotor is made of 17 blades and the OGV number is 23. Three OGV blades are thicker than other ones for mechanical reasons. The duct surface pressure is acquired on 48 Bruel & Kjaer ¼'' microphones distributed on a double ring array as on Figure 8. The flush-mounted microphones are calibrated using a procedure described in [12]. The sampling frequency is 25600 Hz, the acquisition duration is 10 s. Each FFT block is made of 2560 samples with an overlap of 50% and a Hanning window.

Figure 8: Pictures of the ducted fan test bench.

Results and Discussion

The magnitude and angle of the measured raw CSM are displayed on Figure 9 at 1200 Hz for illustration. It can be seen that the autospectra are indeed higher than the cross-spectra by an order of magnitude, making the denoising step mandatory. The output of the MD technique applied on the noisy raw CSM is displayed on Figure 9 as a modal spectrum plot. Each mode is especially powerful just above its cut-on frequency (at 1172 Hz, modes [1,1] and [-1,1] lie 5 dB higher than mode [0,1]) The 1st blade passing frequency is located around 2830 Hz at which modes [3,1] and [-3,1] are the most powerful contributors. Note that a subharmonic tonal noise is visible around 900 Hz which corresponds roughly to a third of the 1st BPF. It could be due to the three thick stator blades which constitute a violation of the classical Tayler & Sofrin law. At last it is seen that modes [0,1] and [0,2] clearly dominate over other modes above 3000 Hz.

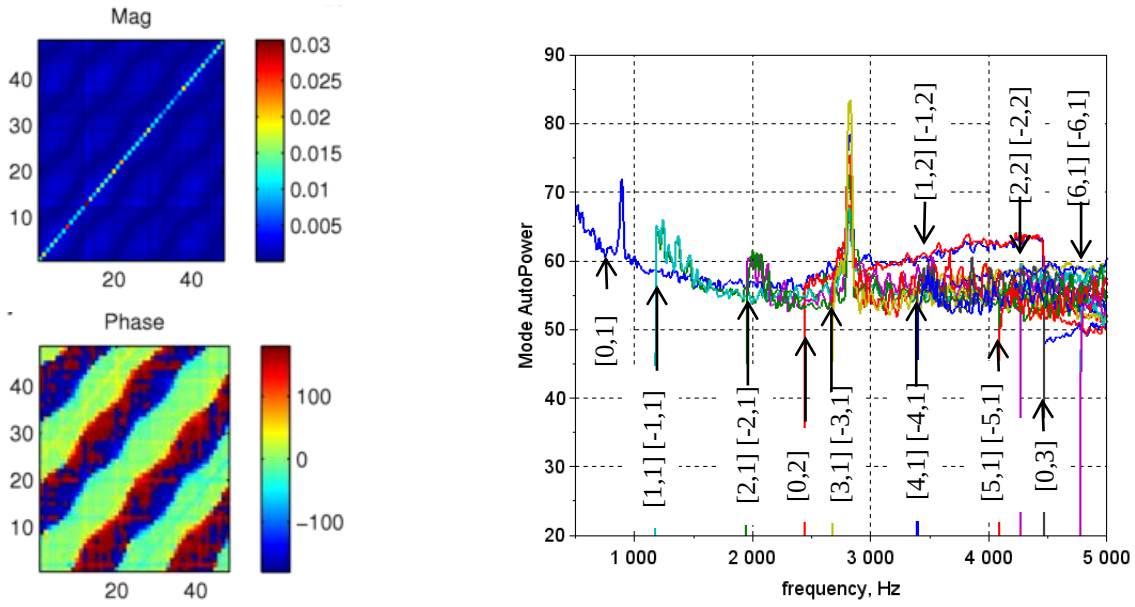

Figure 9: Magnitude (upperleft) and angle (lowerleft) of the raw CSM at 1200 Hz; right: mode spectra for the ducted fan test at 10 000 rpm with the raw noisy CSM.

After the denoising step using the DR or the SLRD technique, the modal spectra are displayed on Figure 10. Again, each mode is powerful just above its cut-on frequency, but this effect is more pronounced on Figure 10 than on Figure 9: at 1172 Hz, modes [1,1] and [-1,1] are 10 dB higher than mode [0,1]. It is considered that denoising enhances the dynamic range of the MD method and thus allow to capture lower levels of less powerful modes. Modes [0,1] and [0,2] are not seen to be predominant above 3000 Hz. This effect was then an artifact of the pseudo-noise contamination. Comparing the DR and the SLRD techniques, it can be seen that SLRD leads 'cleaner' results since the mode spectra are less oscillating against the frequency. Otherwise the modes amplitudes are of the same order of magnitude using both techniques.

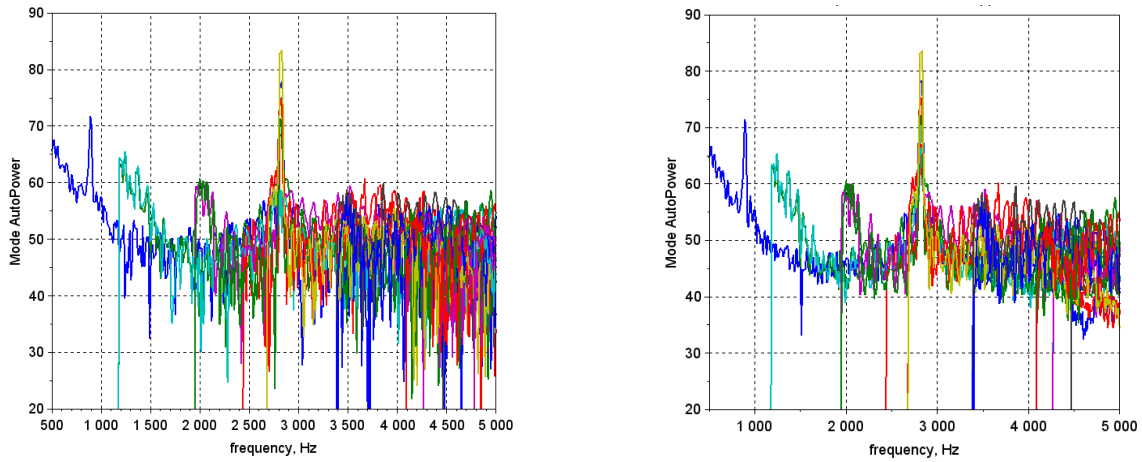

Figure 10: Mode spectra for the ducted fan test at 10 000 rpm with cleaned CSM. Left: DR denoising technique; right: SLRD denoising technique.

CONCLUSIONS

In this paper, different methods are proposed to remove the contribution of a turbulent boundary layer from parietal pressure array measurements in a duct. Two methods are giving very encouraging results, the DR and the SLRD, even if the numerical simulations have shown some limitations: the identification of non-physical CSM (coherences potentially greater than unity) with the former, and an overestimation of modal coherences with the latter. However, it is shown numerically and experimentally that these denoising approaches enhance the modal identification results, improving significantly the dynamic range of the method.

ACKNOWLEDGMENTS

This work is part of the SEMAFOR project, supported by the FRAE. It was performed within the framework of the Labex CeLyA of Université de Lyon, operated by the French National Research Agency (ANR-10-LABX-0060/ ANR-11-IDEX-0007), and the Labcom P3A (ANR-13-LAB2-0011-01).

BIBLIOGRAPHY

[1] L. Enghardt, L. Neuhaus, and C. Lowis, "Broadband sound power determination in flow ducts," in *10th AIAA/CEAS Aeroacoustics Conference*, Manchester, 2004.

[2] F. O. Castres and P. F. Joseph, "Experimental investigation of an inversion technique for the determination of broadband duct mode amplitudes by the use of near-field sensor arrays," *J. Acoust. Soc. Am.*, vol. 122, pp. 848-859, 2007.

[3] J. Y. Chung, "Rejection of flow noise using a coherence function method," *J. Acoust. Soc. Am.*, vol. 62, no. 2, pp. 388-395, 1977.

[4] J. Bulté, "Acoustic Array Measurements in Aerodynamic Wind Tunnels : A Subspace Approach for Noise Suppression," in *13th AIAA/CEAS Aeroacoustics Conference*, Rome, 2007.

[5] B. Arguillat, D. Ricot, and C. a. R. G. Bailly, "Measured wavenumber: Frequency spectrum associated with acoustic and aerodynamic wall pressure fluctuations," *J. Acoust. Soc. Am.*, vol. 128, pp. 1647-1655, 2010.

[6] P. Druault, A. Hekmati, and D. Ricot, "Discrimination of acoustic and turbulent components from aeroacoustic wall pressure field," *J. Sound Vib.*, vol. 332, no. 26, pp. 7257-7278, 2013.

[7] M. E. Goldstein, *Aeroacoustics*. McGraw-Hill, 1976.

[8] S. Boyd and J. Dattorro, "Alternating projections," *Lecture notes of EE 392 o, Stanford University*, 2003.

[9] L. Yu, J. Antoni, and Q. Leclère, "Recovering phase relationships between non-synchronous," in *Proceedings of ISMA 2014*, Leuven, Belgium, 2014.

[10] J. Wright, A. Ganesh, S. Rao, and Y. Ma, "Robust principal component analysis: Exact recovery of corrupted low-rank matrices via convex optimization," *in Proceedings of the Conference on Neural Information Processing Systems (NIPS)*, 2009.

[11] L. Yu, J. Antoni, and Q. Leclère, "Combined Regularization Optimization For Separating Transient Signals From Strong Noise In Rolling Element Bearing Diagnosis," in *Proceedings of Surveillance 7*, Chartres, France, 2013.

[12] A. Finez, R. Leneveu, C. Picard, and P. Souchotte, "In-Duct Acoustic Source Detection Using Acoustic Imaging Techniques," in *AIAA*, Berlin, 2013-2254.

[13] T. Mueller, *Aeroacoustic Measurements*. Springer, 2002.